RESEARCH ARTICLE

Theoretical spectroscopic study of acetyl (CH_3CO), vinoxy (CH_2CHO), and 1-methylvinoxy (CH_3COCH_2) radicals. Barrierless formation processes of acetone in the gas phase [version 1; peer review: awaiting peer review]

Hamza El Hadki[1], Victoria Guadalupe Gámez[2], Samira Dalbouha[1,3], Khadija Marakchi[1], Oum Keltoum Kabbaj[1], Najia Komiha[1], Miguel Carvajal[4,5], Maria Luisa Senent Diez[2]

[1]Laboratoire de Spectroscopie, Modélisation Moléculaire, Matériaux, Nanomatériaux, Eau et Environnement, LS3MN2E/CERNE2D, Faculté des Sciences Rabat, Université Mohammed V, Rabat, BP1014, Morocco
[2]Departamento de Química y Física Teóricas, IEM-CSIC, Unidad Asociada GIFMAN, CSIC-UHU, Madrid, 28006, Spain
[3]Equipe de recherche : Matériaux et Applications Environnementales, Laboratoire de Chimie Appliquée et Environnement, Département de chimie, Faculté des Sciences d'Agadir, Université Ibn Zohr, Agadir, B.P 8106, Morocco
[4]Departamento de Ciencias Integradas, Centro de Estudios Avanzados en Física, Matemática y Computación; Unidad Asociada GIFMAN, CSIC-UHU, Universidad de Huelva, Huelva, 21071, Spain
[5]Instituto Universitario Carlos I de Física Teórica y Computacional, University of Granada, Granada, Spain

v1 **First published:** 30 Sep 2021, **1**:116
https://doi.org/10.12688/openreseurope.14073.1
Latest published: 30 Sep 2021, **1**:116
https://doi.org/10.12688/openreseurope.14073.1

Abstract

Background: Acetone is present in the earth´s atmosphere and extra-terrestrially. The knowledge of its chemical history in these environments represents a challenge with important implications for global tropospheric chemistry and astrochemistry. The results of a search for efficient barrierless pathways producing acetone from radicals in the gas phase are described in this paper. The spectroscopic properties of radicals needed for their experimental detection are provided.

Methods: The reactants were acetone fragments of low stability and small species containing C, O and H atoms. Two exergonic bimolecular addition reactions involving the radicals CH_3, CH_3CO, and CH_3COCH_2, were found to be competitive according to the kinetic rates calculated at different temperatures. An extensive spectroscopic study of the radicals CH_3COCH_2 and CH_3CO, as well as the CH_2CHO isomer, was performed. Rovibrational parameters, anharmonic vibrational transitions, and excitations to the low-lying excited states are provided. For this purpose, RCCSD(T)-F12 and MRCI/CASSCF calculations were performed. In addition, since all the species presented non-rigid properties, a variational procedure of reduced dimensionality was employed to explore the far infrared region.

Open Peer Review

Reviewer Status *AWAITING PEER REVIEW*

Any reports and responses or comments on the article can be found at the end of the article.

Results: The internal rotation barriers were determined to be V_3 =143.7 cm^{-1} (CH_3CO), V_2=3838.7 cm^{-1} (CH_2CHO) and V_3=161.4 cm^{-1} and V_2=2727.5 cm^{-1} (CH_3COCH_2).The splitting of the ground vibrational state due to the torsional barrier have been computed to be 2.997 cm^{-1}, 0.0 cm^{-1}, and 0.320 cm^{-1}, for CH_3CO, CH_2CHO, and CH_3COCH_2, respectively.
Conclusions: Two addition reactions, $H+CH_3COCH_2$ and CH_3+CH_3CO, could be considered barrierless formation processes of acetone after considering all the possible formation routes, starting from 58 selected reactants, which are fragments of the molecule. The spectroscopic study of the radicals involved in the formation processes present non-rigidity. The interconversion of their equilibrium geometries has important spectroscopic effects on CH_3CO and CH_3COCH_2, but is negligible for CH_2CHO.

Keywords
acetone, CH3CO, CH2CHO, CH3COCH2, radical, spectrum, barrierless, LAM

This article is included in the Excellent Science gateway.

Corresponding author: Maria Luisa Senent Diez (ml.senent@csic.es)

Author roles: El Hadki H: Data Curation, Investigation; **Gámez VG**: Data Curation, Formal Analysis, Investigation, Resources, Software, Visualization; **Dalbouha S**: Data Curation, Formal Analysis, Investigation, Visualization; **Marakchi K**: Conceptualization, Data Curation, Investigation, Validation; **Kabbaj OK**: Formal Analysis, Supervision, Validation; **Komiha N**: Conceptualization, Formal Analysis, Funding Acquisition, Investigation, Project Administration, Validation; **Carvajal M**: Conceptualization, Funding Acquisition, Investigation, Methodology, Project Administration, Validation, Writing – Original Draft Preparation; **Senent Diez ML**: Conceptualization, Formal Analysis, Funding Acquisition, Investigation, Methodology, Project Administration, Resources, Software, Supervision, Writing – Original Draft Preparation, Writing – Review & Editing

Competing interests: No competing interests were disclosed.

Grant information: This project has received funding from the European Union's Horizon 2020 research and innovation programme under the Marie Skłodowska-Curie grant agreement No 872081. This work was also supported by the Ministerio de Ciencia, Innovación y Universidades of Spain through the grants EIN2019-103072 and FIS2016-76418-P; the CSIC i-coop+2018 program under the grant number COOPB20364; the CTI (CSIC) and CESGA and to the "Red Española de Computación" for the grants AECT-2020-2-0008 and RES-AECT-2020-3-0011 for computing facilities. MC also acknowledges the financial support from the Spanish National Research, Development, and Innovation plan (RDI plan) under the project PID2019-104002GB-C21 and the Consejería de Conocimiento, Investigación y Universidad, Junta de Andalucía and European Regional Development Fund (ERDF), Ref. SOMM17/6105/UGR.
The funders had no role in study design, data collection and analysis, decision to publish, or preparation of the manuscript.

How to cite this article: El Hadki H, Gámez VG, Dalbouha S *et al.* **Theoretical spectroscopic study of acetyl (CH_3CO), vinoxy (CH_2CHO), and 1-methylvinoxy (CH_3COCH_2) radicals. Barrierless formation processes of acetone in the gas phase [version 1; peer review: awaiting peer review]** Open Research Europe 2021, **1**:116 https://doi.org/10.12688/openreseurope.14073.1

First published: 30 Sep 2021, **1**:116 https://doi.org/10.12688/openreseurope.14073.1

Plain language summary

In addition to its industrial applications, acetone (CH_3COCH_3), the smallest ketone, is present in gas phase environments such as the earth´s atmosphere and extraterrestrial sources. The knowledge of its chemical history in these environments, as well as that of other volatile molecular species, represents a challenge with important implications for global tropospheric chemistry. Organic radicals can play important roles in the chemical evolution.

In this paper gas phase barrierless processes and the corresponding properties were studied at different temperatures. Probable exergonic bimolecular addition processes, which reactants are acetone fragments or small neutral species observed in the gas phase sources containing C, O and H atoms, were described. In addition, this paper is devoted to the theoretical spectroscopic study of three radicals: the acetyl radical (CH_3CO), the vinoxy radical (CH_2CHO), and the 1-methylvinoxy radical (CH_3COCH_2). The three systems were acetone fragments and potential reactants. Our main objective is to provide the theoretical point of view to help further spectroscopic studies of these not-yet-fully characterized species that can play important roles in the gas phase chemistry.

Introduction

In addition to its industrial applications, acetone (CH_3COCH_3), the smallest ketone, is present in gas phase environments such as the earth´s atmosphere and the interstellar medium[1–5]. The knowledge of its chemical history in these environments, as well as that of other volatile molecular species, represents a challenge with important implications for global tropospheric chemistry and astrochemistry. Organic radicals can play important roles in the chemical evolution of the terrestrial atmosphere and extra-terrestrial gas phase sources.

Atmospheric acetone arises from both natural and anthropogenic sources[1,2]. It is naturally produced by vegetation that emits large quantities of nonmethane organic compounds. In the troposphere, these biogenic compounds can undergo photolysis and react with OH and NO_3 radicals, and ozone, resulting in the formation of oxygenated products such as ketones[2,5,6]. On the other side, acetone is a major source of hydrogen oxide radicals (HO_x) and peroxyacetyl nitrate through photolysis[2,6]. Decomposition of acetone can occur in the presence of OH to produce radicals such as CH_3COCH_2[7]. The OH-initiated oxidation of acetone in the presence of NO in air has been shown to form the acetonoxy radical [CH_3COCH_2O], which undergoes rapid decomposition under atmospheric conditions to form HCHO and CH_3CO[1].

Acetone was the first ten-atom molecule to be detected in the interstellar medium[4,5]. Recently, it has been observed in the gas phase in various extraterrestrial environments[8,9]. It is generally accepted that organic compounds are formed in the interstellar medium on ice mantles, although the possibility of gas phase processes is not ignored[10]. At the temperatures and pressures of the interstellar medium, barrierless processes can be competitive with respect to those involving ice mantles[11]. Barrierless processes involve low stability species such as radicals, charged or unsaturated molecules[11].

Following the same methodology employed in a previous work[11], for this paper, gas phase barrierless processes and the corresponding kinetic rates were studied at different temperatures. Probable exergonic bimolecular addition processes, the reactants which are acetone fragments or small neutral species observed in the gas phase sources containing C, O and H atoms, are described. In addition, this paper is devoted to the theoretical spectroscopic study of three radicals: the acetyl radical (CH_3CO), the vinoxy radical (CH_2CHO), and the 1-methylvinoxy radical (CH_3COCH_2). The three systems were acetone fragments and potential reactants. Our main objective is to provide perspective from the *ab initio* calculations and to help further spectroscopic studies of these three, not yet fully characterized species that can play important roles in the gas phase chemistry involving organic molecules, such as diacetyl or pyruvic acid[12,13].

The rotational spectra of CH_3CO and CH_2CHO were measured by Hirota *et al.*[14], Endo *et al.* and Hansen *et al.*[15,16], respectively. As far we know, experimental rotational parameters are not available for CH_3COCH_2.

The vibrational spectra of the CH_3CO, CH_2CHO, and CH_3COCH_2 radicals were studied in Ar matrices by Jacox[17], Shirk *et al.*[18], and Lin *et al.*[19], respectively, whereas Das and Lee[20] addressed the infrared spectrum of CH_3CO in solid p-H_2. In the gas phase, previous measurements corresponding to CH_2CHO[21–27] and CH_3COCH_2[28] are accessible, whereas for CH_3CO experimental vibrational data in the gas phase are unavailable.

Low-lying electronic transitions were previously measured for the three radicals. The CH_3CO radical photodecomposes into CH_3+CO in the visible region[17]. The ground electronic state presented a doublet

multiplicity character. In addition, three excited electronic doublet states have been explored[29–32]. Band centers were determined to lie at 2.3 eV[29] and in the 200-240 nm (5.1-6.2 eV) region[30]. Maricq *et al.*[31] observed bands at 217 nm (2.3 eV) and in the 240-280 nm (4.4-5.1 eV) region, which were confirmed by Cameron *et al.*[32]. For the CH_2CHO isomer, the A(A")←X(A") and B(A")←X(A") transitions has been centered at 1.0 eV[26,33,34] and at 3.6 eV[22–25,33,35,36] using different experimental techniques. The B(A")←X(A") transition of CH_3COCH_2 was found at 3.4 eV by Williams *et al.*[37,38] who also provided internal rotation barriers. To our knowledge, all the previous experimental data concerned doublet states. No information is available concerning quartet states. Since one of our objectives was to localize the excited states, all the previous data is summarized with our results.

Theoretical techniques have also been applied to the study of the three radicals[39–41]. Mao *et al.*[39] have determined vertical excitation energies to four excited doublet states of CH_3CO using multireference single and double excitation configuration interaction. The work of Yamaguchi *et al.*[40] focused on the CH_2CHO, and CH_3COCH_2 radicals.

For this new paper, we tackle to different spectroscopic properties with special attention to the far infrared region, relevant for the interpretation of rovibrational spectra. This new paper is organized as follows: The "computational tools" section under the Methods contains information about the electronic structure computations and computer codes. The next section presents the results and the discussion about the barrierless formation processes of acetone and the corresponding kinetic rates; the spectroscopic characterization of the radicals using two different procedures (one of them suitable for species with large amplitude vibrations and the far infrared region), is explored. Our recent studies of acetone[42] and the CH_3OCH_2 radical[43] are examples of this last procedure. Finally, the conclusions are drawn.

Methods

Computational tools

Different levels of electronic structure theory were combined taking into consideration the computational requirements of the reactive processes and the spectroscopic studies.

Formation processes. The search for the possible barrierless formation processes was performed using the Searching Tool for Astrochemical Reactions (STAR) online tool[44]. This statistical tool contains a broad and comprehensive molecular database. Implemented algorithms search for all the likely combinations of reactants leading to a specific molecular species. The processes producing the desired molecule and some subproducts are automatically rejected if the viability of these last species cannot be confirmed according to the Gibbs free energy. The viability is considered confirmed when species are listed in the data base. The corresponding minimum energy paths were computed using the density functional theory (DFT)[45] and the 6-311+G(d,p) basis set[46] as it is implemented in the GAUSSIAN 16 software[47]. The thermochemical properties were determined by optimizing the geometry with the CBS-QB3 procedure[48], a complete basis set model implemented in GAUSSIAN modified for the use of the B3LYP hybrid density functional. The corresponding kinetic rate constants were computed using POLYRATE version 2017 software[49].

Spectroscopic and geometrical properties. The ground electronic state structure of the three radicals and the corresponding harmonic frequencies were computed using explicitly correlated coupled cluster theory with single and double substitutions, augmented by a perturbative treatment of triple excitations, RCCSD(T)-F12[50,51] implemented in MOLPRO version 2012.1[52]. The default options and a basis set denoted by AVTZ-F12, were employed. AVTZ-F12 contains the aug-cc-pVTZ (AVTZ)[53] atomic orbitals, the corresponding functions for the density fitting, and the resolutions of the identity. The core-valence electron correlation effects on the rotational constants were introduced using RCCSD(T)[54] and the cc-pCVTZ basis set (CVTZ)[55].

The three radicals can be defined as nonrigid molecules because they show large amplitude motions that interconvert different minima of the potential energy surface (PES). Then, two different theoretical models were combined to determine the spectroscopic parameters, vibrational second order perturbation theory (VPT2)[56] implemented in GAUSSIAN, and a variational procedure of reduced dimensionality which is detailed in our papers[57–59].

If VPT2 is applied, a unique minimum is postulated to exist in the potential energy surfaces, the radicals are assumed to be semi-rigid and all the vibrations are described as small displacements around the equilibrium geometry. For CH_3CO, CH_2CHO, and CH_3COCH_2, anharmonic spectroscopic frequencies were obtained

from anharmonic force fields, computed using second order Møller-Plesset theory (MP2) and the VQZ, VQZ, and AVTZ basis sets[52], respectively.

If the variational procedure is applied, the non-rigidity is taken into account and the minimum interconversion is considered implicitly. For this purpose, RCCSD(T)-F12/AVTZ potential energy surfaces were computed, and later on they were vibrationally corrected at the MP2/VQZ, MP2/VQZ, and MP2/AVTZ level of theory, respectively.

Vertical excitation energies to the excited electronic states were computed using MRCI/CASSCF theory[60,61]. For the two small radicals, the active space was constructed with eight a' and four a" orbitals and 13 electrons. The five a' internal orbitals, doubly occupied in all the configurations, were optimized. In the case of CH_3COCH_2, the active space was built using nine a' and four a" orbitals and fifteen electrons, whereas eight a' orbitals were optimized but they were doubly occupied in all the configurations.

Results and discussion

Barrierless formation processes of acetone: the function of radicals

In the gas phase, efficient reactions for competing with formation processes on ice surfaces are those which follow barrierless pathways and involve low stability species. To establish some limits to the present work, we choose the set of reactants shown in Table 1. In principle, they obey the following conditions: (1) they enclose the atomic elements H, C, and O constituents of acetone; (2) they contain at most eleven atoms, as the objective is to select chemical routes of increasing molecular complexity; (3) they have been detected in the gas phase of the ISM or, at least, they are listed as probably detectable species. We detail this procedure in our previous paper on the $C_3O_3H_6$ isomers[11].

All the possible chemical routes starting from the selected reactants were automatically generated by the STAR software[44]. This statistical tool contains a broad and comprehensive molecular database. Implemented algorithms search for all likely combinations of reactants leading to a specific molecular species. The processes producing the desired molecule and some by-products are automatically rejected if the viability of these last species cannot be confirmed. The tool selects the exergonic processes for which the exchange of Gibbs free energies is negative ($\Delta G < 0$). The selected processes must occur following a limited number of steps. The number of steps is considered to concur with the sum of breaking and forming bonds. To quantify them, the maximum number of necessary elementary steps (MNES) parameter is defined.

In principle, 75 exergonic processes are derived from STAR. For all of them, ΔG was computed by optimizing the geometry using the CBS-QB3 procedure[48]. Fourteen final exergonic reactions for which MNES < 3 were found, but only two of them could be considered as barrierless processes (see Table 2). Energy profiles proving these findings were computed at the M05-2X/6-311+G(d,p) level of theory[45,46]. They represent minimum energy paths.

Table 1. List of selected reactants (N_a = number of atoms).

N_a	*Reactants*
1	$^{\bullet}H$
2	H_2; $^3O_2$; C_2; $OH^{\bullet}$; $CH^{\bullet}$; OH^+; CH^+; $CO^{\bullet+}$; CO
3	C_3; HOC^+; $C_2H^{\bullet}$; H_2O; C_2O; $H_2O^{\bullet+}$; $^3CH_2$; H_3^+; CO_2; HCO^+; $HCO^{\bullet}$
4	$HOCO^+$; l-$C_3H^{\bullet}$; $CH_3^{\bullet}$; H_2CO; HCOH; C_3O; $HCOO^{\bullet}$; C_2H_2; $HOCO^{\bullet}$; H_3O^+; HCCO
5	$^{\bullet}CH_2OH$; $C_4H^{\bullet}$; $CH_3O^{\bullet}$; C_4H^-; HCOOH; CH_4; l-C_3H_2; CH_2CO
6	C_2H_4; $CH_3CO^{\bullet}$; CH_3OH;$^{\bullet}CH_2CHO$; HC_2CHO; H_2C_4; HC_4H
7	CH_3CHO; CH_2CHOH; CH_3C_2H
8	CH_2CHCHO; $CH_3OCH_2^{\bullet}$; CH_3CHOH
9	CH_3C_4H; CH_3CH_2OH; $CH_3COCH_2^{\bullet}$; CH_3CCH_3; CH_3CHCH_2

Table 2. Rate constants ($cm^3 molecule^{-1} s^{-1}$).

	Reaction	200K		298K	500K	1000K
		CVT	μVT	CVT	CVT	CVT
1	$H^{\bullet} + CH_3COCH_2 \rightarrow CH_3COCH_3$	6.3E-21	0.0E+00	2.6E-17	8.2E-15	5.2E-13
2	$CH_3^{\bullet} + CH_3CO^{\bullet} \rightarrow CH_3COCH_3$	6.0E-21	0.0E+00	2.4E-17	2.3E-14	3.3E-12

The kinetic rate constants of the processes are summarized in Table 2. They were evaluated using the single-faceted variable-reaction-coordinate variational transition state theory (VRC-VTST)[62,63] implemented in POLYRATE[49]. The rate constants obey the following equation:

$$k(T,s) = \frac{\hbar^2}{2\pi} g_e \frac{\sigma_1 \sigma_2}{\sigma^{\neq} Q_1 Q_2} \left(\frac{2\pi}{\mu k_B T} \right)^{3/2} \int dE\, e^{-E/K_B T}\, dJ\, N(E,J,s) \quad (1)$$

In this equation, s and T denote the reaction coordinate and the temperature, respectively; g_e represents the rate between the electronic partition function of the transition state and the product of the electronic partition function of the two reactants; μ, Q_1 and Q_2 designate the reduced mass and the rotational partition functions of the reactants. J is the angular momentum quantum number and N (E, J, s) represents the number of allowed states corresponding to the E energy. σ_1, σ_2, and $\sigma^{\neq}$ denote the cross-sections for the two reactants and for the transition states.

The starting points of the rate computation were the M05-2X/6-311+G(d,p) energies, geometries and harmonic fundamentals of reactants and products computed along the pathways. The s reaction coordinate was allowed to vary from 1.8 to 4.2 Å with intervals of 0.2 Å. The rates were computed at fifteen different T (200, 210, 220, 230, 240, 250, 260, 280, 298, 300, 400, 500, 700, 900 and 1000K). The number of allowed states was determined in a Monte Carlo simulation considering all the possible orientations. The rates at 200K (middle point of the interstellar Hot Core temperature range, 100-300K), 298K (room temperature), and 500K, corresponding to the 29 barrierless processes, are shown in Table 2. Rates were computed using the canonical variational transition state theory (CVT), which is the conventional theory. However, as CVT is not recommended for very low temperatures, rates at 200K were also computed using microcanonical variational transition state theory (μVT) with multidimensional semiclassical approximations for tunneling and nonclassical reflection[64,65].

Spectroscopic characterization of CH_3CO, CH_2CHO, and CH_3COCH_2

Ground electronic state: equilibrium structures. The study of the rovibrational properties of acetone and its monosubstituted isotopologues using *ab initio* calculations was the aim of a previous work from some of the authors of the present paper[42]. In this new paper, we attend, using a similar methodology, the structural and spectroscopic parameters of the three radicals, CH_3CO, CH_2CHO, and CH_3COCH_2, involved in acetone gas phase processes.

Table 3 collects the RCCSD(T)-F12/AVTZ structural parameters and the equilibrium rotational constants of the preferred geometries of the three radicals in their ground electronic state. The three geometries can be classified in the C_s point group. The MRCI/CASSCF/AVTZ dipole moment components are also shown. Figure 1 represents those preferred geometries.

The three radicals display internal rotation that interconvert equivalent minima separated by barriers. θ_1 and θ_2 denote the CH_3 and the CH_2 torsional coordinates, respectively. Using RCCSD(T) theory, the energy barriers were computed to be V_3=143.7 cm^{-1} (CH_3CO), V_2=3838.7 cm^{-1}(CH_2CHO), and V_3=161.4 cm^{-1} and V_2=2727.5 cm^{-1} (CH_3COCH_2). A third coordinate, α (the CH_2 wagging) interacts strongly with the CH_2 torsion in two of the three species. Figure 2 represents one-dimensional cuts of the ground electronic state potential energy surfaces that emphasize the torsional barriers.

It could be concluded that in CH_3CO and CH_3COCH_2, the methyl torsional barrier is very low (V_3 <200 cm^{-1}). A complex distribution of the torsional energy levels can be expected. With respect to the CH_2 torsion, the barrier in CH_3COCH_2 is ~0.70 $V_2^{CH2\text{-}CHO}$ and of the same order of magnitude as in CH_3OCH_2[43].

Table 3. RCCSD(T)-F12/AVTZ relative energies (E, E^{ZPVE}, in cm^{-1}), internal rotation barriers (V_3, V_2, in cm^{-1}). Rotational constants (in MHZ), MRCI/CASSCF/AVTZ dipole moment (in D) and equilibrium structural parameters (*distances, in Å, angles, in degrees)* of acetyl, vinoxy, and 1-methylvinoxy radicals.

	CH_3CO[a] (X^2A')	CH_2CHO (X^2A'')	CH_3COCH_2[b] (X^2A'')
E	0.0	2514.2	-
E^{ZPVE}	0.0	2498.8	-
V_2	-	3838.7	2727.5
V_3	143.7	-	161.4
A_e	84134.35	67084.88	10934.76
B_e	9982.57	11456.25	9115.74
C_e	9444.29	9785.20	5128.93
μ_a	0.2423	0.9465	0.5444
μ_b	2.3244	2.6175	1.3272
μ_c	0.0	0.0	0.0
μ	2.3281	2.7834	1.4346
CH_3CO		**CH_2CHO**	
C1C2	1.5116	C1C2	1.4325
O3C1	1.1816	O3C2	1.2290
H4C2	1.0912	H4C2	1.1014
H5C2=H6C2	1.0892	H5C1=H6C1	1.0809
O3C1C2	128.3	O3C2C1	122.8
H4C2C1	110.7	H4C2C1	117.0
H5C2C1=H6C2C1	108.4	H5C1C2	119.0
H4C2C1O3	0.0	H6C1C2	120.9
H5C2C1H4=-H6C2C1H4	121.6		
CH_3COCH_2			
C1C2	1.5129	C2C1O4	121.6
C1C3	1.4467	H5C2C1	109.5
O4C1	1.2291	H6C2C1=H7C2C1	110.2
H5C2	1.0869	C1C3H8	118.1
H6C2=H7C2	1.0917	H9C3H8	119.9
H8C3	1.0803	H5C2C1C3	180.0
H9C3	1.0814	H6C2C1H5= -H7C2C1H5	120.8
C2C1C3	117.9		
a) E=-152.989163 a.u.; b) E=-192.240093 a.u.			

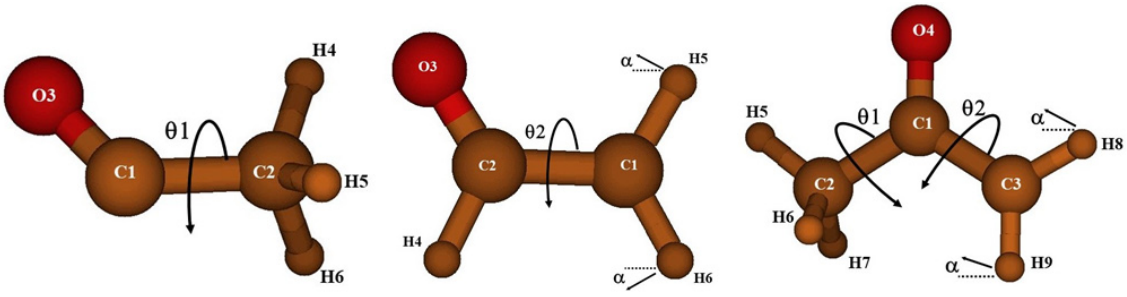

Figure 1. The preferred geometries of the CH_3CO, CH_2CHO, and CH_3COCH_2 radicals.

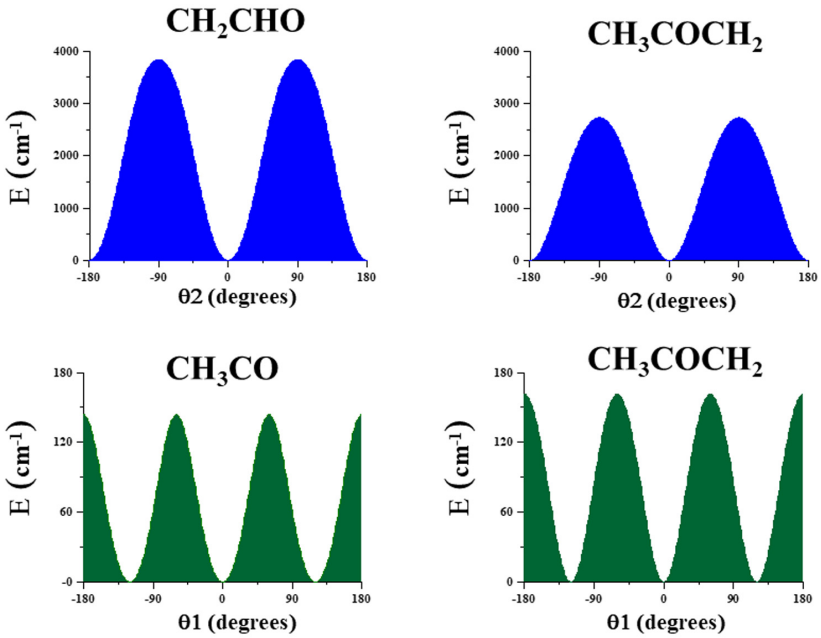

Figure 2. Internal rotation barriers.

Excited electronic states. Previous theoretical and experimental works resolved doublet multiplicity character of the electronic ground states. Nevertheless, using MRCI/CASSCF/AVTZ theory, we have identified the lowest excited electronic states to assure a clean enough ground electronic state to apply the used rovibrational models. Results are shown in Table 4 and were compared with previous experimental data[22–26,29,31,33–38] or data from theoretical works[39,40].

The first excited electronic state of CH_3CO and CH_3COCH_2 is a doublet state lying around 2 eV above the ground state. Vibronic effects are expected in the spectral region of the ground electronic state studied in this work. In the case of the CH_3CO radical, the computed value is in good agreement with experiments[29]. For CH_2CHO, the vertical excitation to the first excited state was computed to be 1.4 eV in agreement with the experimental value of 1.0 eV[26,33,34]. As a consequence, the first excited state can perturb the region of the H-stretching overtones. For the three species, the following higher excited states (doublets and quartets) lie over 4 eV.

Ground electronic state rovibrational properties. The vibrational energy levels have been obtained using the following formula:

$$E = \sum_i \omega_i^{RCCSD(T)-F12}\left(v_i + \frac{1}{2}\right) + \sum_{i \geq j} x_{ij}^{MP2}\left(v_i + \frac{1}{2}\right)\left(v_j + \frac{1}{2}\right) \quad (2)$$

Table 4. Vertical excitation energies to the low-lying electronic states (in eV) computed with MRCI/CASSCF/AVTZ.

CH_3CO[a]			CH_2CHO[b]			CH_3COCH_2[c]		
	Calc.	Previous works		Calc.	Previous works		Calc.	
X^2A'	0.0	-	X^2A''	0.0		X^2A''	0.0	
A^2A''	2.4	2.33[29] 2.6[39]	A^2A'	1.4	1.0[26,33,34]	A^2A'	2.2	
B^2A'	6.2	5.8[30] (4.4-5.2)[31] 4.9[39]	B^2A''	4.4	3.57[22–25,33,35,36] 3.4[40]	a^4A'	5.0	
$a\ ^4A''$	6.3		a^4A'	4.9		B^2A''	5.7	3.4[37,38] 3.5[40]
b^4A'	6.7		C^2A'	5.4		b^4A''	6.4	
C^2A''	7.0	6.7[39]	b^4A''	7.2		C^2A'	6.8	

a) 29 Visible Absorption Spectrum; 30; Flash photolysis and kinetic spectroscopy; 31 Ultraviolet spectrum ; 39 MR(SD)CI calculations;

b) 22–25,36 Laser induced fluorescence; 26,34 Photoelectron spectroscopy; 33 Photochemical modulation spectroscopy; 35 Photodissociation spectroscopy; 40 MRCISD+Q/cc-pVDZ

c) 37,38 laser induced fluorescence; 40 MRCISD+Q/cc-pVDZ

where ω_i represents the RCCSD(T)-F12 harmonic fundamentals and x_{ij} are the MP2 anharmonic constants. These last values were computed using VPT2 theory and harmonic force fields MP2/AVQZ (in the case of the small radicals) and MP2/AVTZ (in the case of CH_3COCH_2). In Table 5, the computed fundamentals are compared with previous measured values in Ar[16–18] and p-H_2[20] matrices, and in the gas phase[21–28].

The ground vibrational state rotational constants and the centrifugal distortion constants are shown in Table 6. The rotational constants were computed using the RCCSD(T)-F12 equilibrium parameters of Table 3 and the following equation, proposed and verified in previous studies[42,65–67]:

$$B_0 = B_e\,(\text{RCCSD(T)-F12/AVTZ}) + \Delta B_e^{\text{core}}\,(\text{RCCSD(T)/CVTZ}) + \Delta B_{\text{vib}}\,(\text{MP2/AVnZ}) \quad (3)$$

Here, ΔB_e^{core} takes into account the core-valence-electron correlation effect on the equilibrium parameters. It can be evaluated as the difference between B_e(CV) (calculated by correlating both core and valence electrons) and B_e(V) (calculated by only correlating the valence electrons). ΔB_{vib} represents the vibrational contribution to the rotational constants derived from the VPT2 α_{ir} vibration-rotation interaction parameters.

Rotational parameters of CH_3CO were compared with the experimental values of Hirota *et al.*[14], whereas those of CH_2CHO were compared with the data of Endo *et al.*[15]. For this second radical, the agreement between computed and measured rotational constants is excellent (A_0^{CAL}-A_0^{EXP} = 95.3 MHz, B_0^{CAL}-B_0^{EXP} = -1.7 MHz, and C_0^{CAL}-C_0^{EXP} = 3.2 MHz). However, for CH_3CO, the concurrence is also excellent for B_0 and C_0, but the A_0 result is outside tolerance limits (A_0^{CAL}-A_0^{EXP} = 1147.5 MHz, B_0^{CAL}-B_0^{EXP} = -3.4 MHz, and C_0^{CAL}-C_0^{EXP} = 0.5 MHz). Generally, for many molecules, the computed B_0 and C_0 using Equation (3) are more accurate than A_0. However, the difference expressed as A_0^{CAL}-A_0^{EXP} = 1147.5 MHz is too large in comparison to what was expected. Since the three rotational constants were computed simultaneously, the error could be derived from the experiments and from the effective Hamiltonian used for assignments. For methyl isocyanate[68], we found a similar situation, where it is proven that previous experimental works provided very contradictory A_0 constants.

Table 5. Anharmonic fundamentals[a,b,c] (in cm^{-1}).

CH_3CO				
			Calc.	**Obs.[d] [Ref]**
ν(a')	ν_1	CH_3 st	2988	2989.1 (19)[20]
	ν_2	CH_3 st	2919	2915.6(29)[20]
	ν_3	CO st	**1900**	1880.5 (100)[20]; 1875[17]; 1842[18]
	ν_4	CH_3 b	1427	1419.9(80)[20]; 1420[17]
	ν_5	CH_3 b	1331	1323.2(109)[20]; 1329[17,18]
	ν_6	HCC b	**1021**	
	ν_7	CC st	833	836.6(45)[20]
	ν_8	OCCb	464	468.1(28)[20]
ν(a'')	ν_9	CH3 st	**2997**	2990.3(42)[20]
	ν_{10}	CH_3 b	1429	1419.9(80)[20]
	ν_{11}	CH_3 b	**931**	
	ν_{12}	CH_3 tor	82	
CH_2CHO				
ν(a')	ν_1	CH st	3133	
	ν_2	CH st	3035	
	ν_3	CH st	**2813**	2827.91[21]
	ν_4	CCO st	**1465**	1528[22–26]
	ν_5	CH_2 b	**1435**	1486[25]
	ν_6	OCH b	**1365**	24,25
	ν_7	CC st	1132	1143[22,23,25–27]
	ν_8	CC st	950	957[25]
	ν_9	CCO b	495	22–23,25–27
ν(a'')	ν_{10}	H_4 wag	954	703[25]
	ν_{11}	CH_2 wag	729	557[25]
	ν_{12}	CH_2 tor	402	402(4)[25]
CH_3COCH_2				
ν(a')	ν_1	CH_2 st	3145	
	ν_2	CH_3 st	2024	
	ν_3	CH_2 st	3040	
	ν_4	CH_3 st	**2927**	
	ν_5	CO st	**1541**	1554.1[16], 1558.9[16]
	ν_6	CH_3 b	**1449**	
	ν_7	CH_2 b	**1440**	1419.32[16]
	ν_8	CH_3 b	1365	1377.51[16]
	ν_9	CCH b	1243	1247[28]
	ν_{10}	CCH b	1051	

CH_3COCH_2				
			Calc.	Obs.[d] [Ref]
	ν_{11}	CCH b	910	
	ν_{12}	CC st	813	
	ν_{13}	OCC b	521	515[28]
	ν_{14}	CCCb	385	
ν(a")	ν_{15}	CH_3 st	2971	
	ν_{16}	CH_3 b	**1440**	
	ν_{17}	CH_3 b	1001	
	ν_{18}	CH_2 wag	732	
	ν_{19}	CH_3 b	500	
	ν_{20}	CH_2 tor	343	
	ν_{21}	CH_3 tor	77	

a) st= stretching; b=bending;wag=wagging; tor=torsion.

b) 16–18 Measured in Ar matrix; 20 in pH_2 solid; 21–28 in the gas phase.

c) Emphasized in bold transitions for which important Fermi displacements are predicted.

d) Experimental uncertainties, when available, are given in parentheses in units of the last quoted digit.

Table 6. Vibrational ground state rotational constants (in MHz) and centrifugal distortion constants corresponding to the symmetrically reduced Hamiltonian parameters (III^r representation[a]).

	CH_3CO		CH_2CHO	
	Calc.	Exp.[b]	Calc.	Exp.[c]
A_0	84094.27	82946.73	66773.15	66677.85679(159)
B_0	9952.09	9955.46	11445.40	11447.0460(55)
C_0	9427.41	9426.95	9762.15	9758.9065(53)
Δ_J	0.009448	0.01188 (21)	0.009422	0.0096468(22)
Δ_K	2.756343		1.312964	1.307
Δ_{JK}	0.124574		-0.084559	-0.083045(137)
d_1	-0.000948		-0.002006	0.0021215(101)
d_2	0.000512		-0.000129	0.0384(26)
H_J	0.000041		0.000014	
H_K	0.897964		0.078700	
H_{JK}	-0.001033		-0.000287	
H_{KJ}	-0.630725		-0.006429	
h_1	0.000004		0.000007	
h_2	-0.000014		0.000001	
h_3	0.000001		0.000000	

	CH_3COCH_2			
	Calc.	**Exp.[b]**	**Calc.**	**Exp.[c]**
A_0	10949.35		H_J	0.000024
B_0	9054.05		H_K	-0.000014
C_0	5110.78		H_{JK}	-0.000088
Δ_J	0.010134		H_{KJ}	0.000078
Δ_K	0.004463		h_1	0.000006
Δ_{JK}	-0.013811		h_2	0.000003
d_1	-0.000763		h_3	0.000002
d_2	-0.000596			

a) The z-axis was selected to coincide with the x-Eckart axis in CH_3CO and CH_2CHO, and with the z-Eckart axis in CH_3COCH_2.

b) Computed from the A, (B±C)/2, and D values of Ref. 14.

c) Ref 15.

The far infrared region

For the three radicals, the energy levels corresponding to the large amplitude motions were computed using a variational procedure of reduced dimensionality, where the vibrational coordinates responsible for the non-rigidity were considered to be separable from the remaining vibrations. Then, an adiabatic approximation is applied on the basis of the vibrational energies. Since the method takes into consideration the minimum interconversion describing the tunneling effects in the barriers, it is more suitable for nonrigid species than VPT2, although this last theory provides a useful preliminary depiction. With VPT2, the methyl torsional fundamental of CH_3CO was computed to be 82 cm^{-1} and the fundamental frequency of the central bond torsion of CH_2CHO was found at 402 cm^{-1} (see Table 5). The CH_3COCH_2 radical presents two interacting internal rotations which VPT2 frequencies computed to be 77 cm^{-1} (CH_3 torsion) and 343 cm^{-1} (CH_2 torsion). In principle, models in one-dimension (1D) or two-dimensions (2D) seems sufficient.

However, as we employed a flexible model where the remaining vibrational modes were allowed to be relaxed during the torsions, a third vibrational mode, the CH_2 wagging, must be considered explicitly as it is strongly coupled with the CH_2 torsion. Fermi interactions, predicted using VPT2, show that the separability between the CH_2 wagging and the CH_2 torsion is not suitable. Then, CH_2CHO and CH_3COCH_2 require (at least) to use 2D and a three-dimension (3D) model, respectively. For the most general case, the 3D Hamiltonian for J=0 must be defined as[57–59]:

$$H(\theta_1,\theta_2,\alpha) = -\sum_{i=1}^{3}\sum_{j=1}^{3}\left(\frac{\partial}{\partial q_i}\right)B_{q_iq_j}(\theta_1,\theta_2,\alpha)\left(\frac{\partial}{\partial q_j}\right)+V^{eff}(\theta_1,\theta_2,\alpha) \qquad (4)$$

$$q_iq_j=\theta_1,\theta_2,\alpha$$

where B_{qiqj} (θ_1,θ_2, α) are the kinetic energy parameters[57–59]; the effective potential is the sum of three terms:

$$V^{eff}(\theta_1,\theta_2,\alpha) = V(\theta_1,\theta_2,\alpha) + V'(\theta_1,\theta_2,\alpha) + V^{ZPVE}(\theta_1,\theta_2,\alpha) \qquad (5)$$

Here, $V(\theta_1,\theta_2, \alpha)$ represents the *ab initio* potential energy surface; $V'(\theta_1,\theta_2, \alpha)$ is the Podolsky pseudopotencial and $V^{ZPVE}(\theta_1,\theta_2, \alpha)$ represents the zero point vibrational energy correction[57–59]. For the 1D and 2D model, the corresponding operators depending on θ_1 (CH_3CO) or θ_2 and α (CH_2CHO) can be easily derived

from Equation (4) removing variables. A possible analytical expression for the potential can be the product of a double Fourier series and a Taylor series:

$$V^{eff}(\theta_1,\theta_2,\alpha)=\sum\sum\sum[A_{mnl}\cos(3m\theta_1)\cos(2n\theta_2)\alpha^{21}+A_{m\text{-}nl}\cos(3m\theta_1)\sin(2n+1)\theta_2\,\alpha^{21+1}$$
$$+A_{\text{-}m\text{-}nl}\sin(3m\theta_1)\sin(2n\theta_2)\alpha^{21}+A_{\text{-}mnl}\sin(3m\theta_1)\cos(2n+1)\theta_2\,\alpha^{21+1}] \quad (6)$$
$$m=0,1,2;n=0,1,2;l=0,1,2,3,4$$

Similar expressions can be used for the kinetic parameters. In the most general 3D case, the Hamiltonian symmetry properties correspond to the totally symmetric representation of G_{12}[69], the molecular symmetry group (MSG) of the CH_3COCH_2 radical. Three-dimensional series corresponding to the six representations, four non degenerate A_1', A_1'', A_2' and A_2'', and two double-degenerate, E' and E" are presented in Table 7. The MSG of the radical CH_3CO is G_6 with three irreducible representations, and that of CH_2CHO is G_4 with four irreducible representations A^+, A^-, B^+ and B^- (based on effects of the symmetry operators (56) and E*).

The kinetic parameters and the *ab initio* potential energy surface were determined from a grid of N selected geometries, corresponding to selected values of the independent coordinates. When 1D, 2D, or 3D models are employed, 1, 2 or 3 internal coordinates are frozen at selected values, whereas $3N_a$-7 (1D), $3N_a$-8 (2D) and $3N_a$-9 (3D) (N_a=number of atoms) are allowed to be relaxed in all the calculated N geometries. For the CH_3COCH_2 radical:

a) Geometries corresponding to four values of the H5C2C1C3 dihedral angle (0°, 90, -90° and 180°) were selected. The methyl torsional coordinate is defined as:

$$\theta_1=(H5C2C1C3+H6C2C1C3+H7C2C1C3-360^o)/3$$

For CH_3CO, the angles $H_xC2C1O3$ (x=4,5,6) define the methyl torsional coordinate.

Table 7. Three-dimensional wavefunctions according to MSG G_{12} (m,n,l=0,1,2,..).

A_1'	E_a'
$\cos(3m\theta_1)\cos(2n\theta_2)\,\alpha^{2l}$ $\cos(3m\theta_1)\sin(2n+1)\theta_2\,\alpha^{2l+1}$	$\cos(3m\pm1)\theta_1\cos(2n\theta_2)\,\alpha^{2l}$ $\cos(3m\pm1)\theta_1\sin(2n+1)\theta_2\,\alpha^{2l+1}$
$\sin(3m\theta_1)\sin(2n\theta_2)\,\alpha^{2l}$ $\sin(3m\theta_1)\cos(2n+1)\theta_2\,\alpha^{2l+1}$	$\cos(3m\pm1)\theta_1\sin(2n\theta_2)\,\alpha^{2l}$ $\cos(3m\pm1)\theta_1\cos(2n+1)\theta_2\,\alpha^{2l+1}$
A_2'	**E_b'**
$\cos(3m\theta_1)\sin(2n\theta_2)\,\alpha^{2l}$ $\cos(3m\theta_1)\cos(2n+1)\theta_2\,\alpha^{2l+1}$	$\sin(3m\pm1)\theta_1\sin(2n\theta_2)\,\alpha^{2l}$ $\sin(3m\pm1)\theta_1\cos(2n+1)\theta_2\,\alpha^{2l+1}$
$\sin(3m\theta_1)\cos(2n\theta_2)\,\alpha^{2l}$ $\sin(3m\theta_1)\sin(2n+1)\theta_2\,\alpha^{2l+1}$	$\sin(3m\pm1)\theta_1\cos(2n\theta_2)\,\alpha^{2l}$ $\sin(3m\pm1)\theta_1\sin(2n+1)\theta_2\,\alpha^{2l+1}$
A_1''	**E_a''**
$\cos(3m\theta_1)\sin(2n\theta_2)\,\alpha^{2l+1}$ $\cos(3m\theta_1)\cos(2n+1)\theta_2\,\alpha^{2l}$	$\cos(3m\pm1)\theta_1\sin(2n\theta_2)\,\alpha^{2l+1}$ $\cos(3m\pm1)\theta_1\cos(2n+1)\theta_2\,\alpha^{2l}$
$\sin(3m\theta_1)\cos(2n\theta_2)\,\alpha^{2l+1}$ $\sin(3m\theta_1)\sin(2n+1)\theta_2\,\alpha^{2l}$	$\cos(3m\pm1)\theta_1\cos(2n\theta_2)\,\alpha^{2l+1}$ $\cos(3m\pm1)\theta_1\sin(2n+1)\theta_2\,\alpha^{2l}$
A_2''	**E_b''**
$\cos(3m\theta_1)\cos(2n\theta_2)\,\alpha^{2l+1}$ $\cos(3m\theta_1)\sin(2n+1)\theta_2\,\alpha^{2l}$	$\sin(3m\pm1)\theta_1\cos(2n\theta_2)\,\alpha^{2l+1}$ $\sin(3m\pm1)\theta_1\sin(2n+1)\theta_2\,\alpha^{2l}$
$\sin(3m\theta_1)\sin(2n\theta_2)\,\alpha^{2l+1}$ $\sin(3m\theta_1)\cos(2n+1)\theta_2\,\alpha^{2l}$	$\sin(3m\pm1)\theta_1\sin(2n\theta_2)\,\alpha^{2l+1}$ $\sin(3m\pm1)\theta_1\cos(2n+1)\theta_2\,\alpha^{2l}$

b) The procedure for defining the coordinates involving the CH_2 group comprises 3 ghost atoms, X_p, X_{CL}, and X. X_p and X defining, respectively, the torsional and wagging coordinates assuring the optimization of $3N_a$-8 in CH_2CHO and $3N_a$-9 in CH_3COCH_2 using the available GAUSSIAN[47] and MOLPRO software[52]. Figure 3 shows the distributions of real and ghost atoms in CH_3COCH_2.

During the geometry optimization, X_p and X_{CL} were frozen in the plane defined by the three carbon atoms; C3-X could wag outside the plane formed by C3C1C2 but remained perpendicular to C3-X_p; the C3-X_p and C3-X_{CL} "bonds" stood perpendicular and collinear to C3-C1, respectively; the real atoms H8 and H9 remained in a plane defined by the X, C3, and X_p atoms. Then, the independent α and θ_2 variables and the corresponding selected values were defined as:

$$\alpha = <XC3X_{CL} \ (\alpha = 0^\circ, \pm 15^\circ, \pm 30^\circ, \pm 45^\circ)$$

$$\theta_2 = X_p C3C1C2 \ (\theta_2 = 180^\circ, 150^\circ, 120^\circ, 90^\circ)$$

A similar procedure was used for CH_2CHO.

The linear fit of the N *ab initio* energies to Equation (6) (R^2=0.99999; σ=1.096 cm^{-1} (CH_3COCH_2)) produced $V(\theta_1,\theta_2,\alpha)$. The kinetic parameters $B_{q1q2}(\theta_1,\theta_2,\alpha)$ and the pseudopotential $V'(\theta_1,\theta_2, \alpha)$ were determined using the procedure described in 57 and 58 for the N geometries and fitted to an expansion formally identical to Equation (6). To determine $V^{ZPVE}(\theta_1,\theta_2,\alpha)$, harmonic frequencies were computed in all the N geometries. Details are shown in 56. The expansion coefficients of the effective potential are provided in Table 8. The A_{000} coefficients of the kinetic parameters are shown in Table 9. Figure 4 displays two bidimensional cuts of the 3D-effective potential of CH_3COCH_2. On the left side of the figure, the two coordinates correspond to the CH_3 and CH_2 torsions. On the right side, the two coordinates are those involving the CH_2 group (torsion and wagging).

The energy levels were computed variationally by solving the Hamiltonian of Equation (4), using the symmetry adapted series shown in Table 7 as trial wave functions. Details concerning the classification of the levels computed in 2D and 3D can be found in 11. Table 10 collects the variational energy levels and the transitions computed using VPT2.

In CH_3CO, the A_1/E splitting of the ground vibrational state was evaluated to be 2.997 cm^{-1}, as was expected given the very low torsional barrier (V_3=143.7 cm^{-1}). The methyl torsional fundamental ν_{12} (1←0), computed to be 82 cm^{-1} with VPT2, present two components: 104.265 cm^{-1} (A_2←A_1) and 73.659 cm^{-1} (E←E). Figure 5 can help understand the distributions of levels and subcomponents. Excitation of the low amplitude motions ν_8 (OCC bending), ν_7 (C-C stretching), and ν_{11} (CH_3 deformation) computed using VPT2 were inserted among the ν_{12} excitations, computed variationally.

In CH_2CHO, the two independent fundamentals treated variationally were ν_{12} (1 0←0 0) and ν_{11} (0 1←0 0). Both were computed to be 402 cm^{-1} and 729 cm^{-1} using VPT2. The variational results were ν_{12} =398.436 cm-1 (A^-←A^+, B^-←B^+) and ν_{11} =745.727 cm^{-1} (A^-←A^+, B^-←B^+). The first one was in agreement with the experimental data (402±4 cm^{-1}[35]) whereas large differences with the experimental work (557 cm^{-1}[35]) were observed for the CH_2 wagging. Both works, experimental and theoretical, need to be revisited in the future to establish the wagging mode. The separation between splitting components (in the ground and first vibrational excited

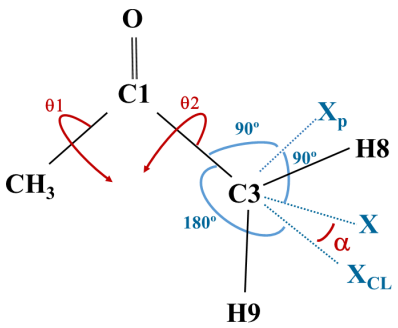

Figure 3. The ghost atoms defining the CH_2 torsional ($X_pC3C1C2$) and the wagging ($XC3X_{CL}$) coordinates, in CH_3COCH_2.

Table 8. Expansion coefficients of the potential energy surfaces (in cm^{-1})[a].

CH_3CO								
A_l		M	A_l		M	A_l		M
66.538		0	-71.867		3	5.329		6
CH_2COH								
A_{nl}	N	L	A_{nl}	N	L	A_{nl}	N	L
2308.050	0	0	0.572	2	2	-4.161	-1	1
-1958.054	2	0	$-0.6x10^{-4}$	2	4	$0.7x10^{-4}$	-1	3
-55.340	4	0	-0.046	4	2	-3.838	-3	1
38.721	6	0	$0.1x10^{-4}$	4	4	$-0.11x10^{-3}$	-3	3
0.589	0	2	0.001	6	2	0.534	-5	1
$0.10x10^{-3}$	0	4	$-0.2x10^{-5}$	6	4	$-0.1x10^{-4}$	-5	3
CH_2COCH_3											
A_{mnl}	N	M	L	A_{mnl}	N	M	L	A_{lmn}	N	M	L
1936.238	0	0	0	$-0.12x10^{-3}$	2	0	4	$0.1x10^{-5}$	4	3	4
-1432.135	2	0	0	0.069	4	0	2	0.008	-1	3	1
-61.140	4	0	0	$-0.4x10^{-4}$	4	0	4	$-0.1x10^{-4}$	-1	3	3
-2.543	6	0	0	0.019	6	0	2	-1.108	-3	3	1
-149.629	0	3	0	$-0.10x10^{-4}$	6	0	4	$-0.5x10^{-4}$	-3	3	3
-0.521	0	6	0	0.062	-1	0	1	-0.033	-5	3	1
0.379	0	0	2	0.007	-1	0	3	$0.5x10^{-4}$	-5	3	3
$0.23x10^{-3}$	0	0	4	2.883	-3	0	1	0.038	-2	-3	2
72.044	2	3	0	0.001	-3	0	3	$-0.1x10^{-4}$	-2	-3	4
-1.843	2	6	0	-0.112	-5	0	1	-0.013	-4	-3	2
-3.507	4	3	0	$-0.5x10^{-4}$	-5	0	3	$0.2x10^{-5}$	-4	-3	4
-0.023	4	6	0	-0.005	0	3	2	-0.056	-6	-3	2
0.378	6	3	0	$0.1x10^{-4}$	0	3	4	$0.3x10^{-4}$	-6	-3	4
0.347	6	6	0	-0.001	0	6	2	0.304	1	-3	1
-73.592	-2	-3	0	-0.023	2	3	2	$0.3x10^{-4}$	1	-3	3
6.280	-4	-3	0	$0.1x10^{-5}$	0	6	4	-1.382	3	-3	1
0.559	2	0	2	0.003	4	3	2	$0.6x10^{-3}$	3	-3	3

a) M=3m; N=2n or 2n+1; L=2l or 2l+1; $M \geq 0 \Rightarrow cos\ 3m\theta_1$; $M < 0 \Rightarrow sin\ 3m\theta_1$; $N \geq 0 \Rightarrow cos\ N\theta_2$; $N < 0 \Rightarrow sin\ N\theta_2$;

Table 9. A_{mnl} (m=0, n=0, l=0) coefficients of the kinetic energy parameters (in cm^{-1})[a].

	$A_{000}(B_{aa})$	$A_{000}(B_{bb})$	$A_{000}(B_{cc})$	$A_{000}(B_{ab})$	$A_{000}(B_{ac})$	$A_{000}(B_{bc})$
CH_3CO	9.8515	-	-	-	-	-
CH_2CHO		11.9647	35.8187	-	-	0.000
CH_3COCH_2	5.7225	9.9603	34.3821	-0.1792	0.000	0.000

a) a=CH_3 torsion; b= CH_2 torsion; c=CH_2 wagging

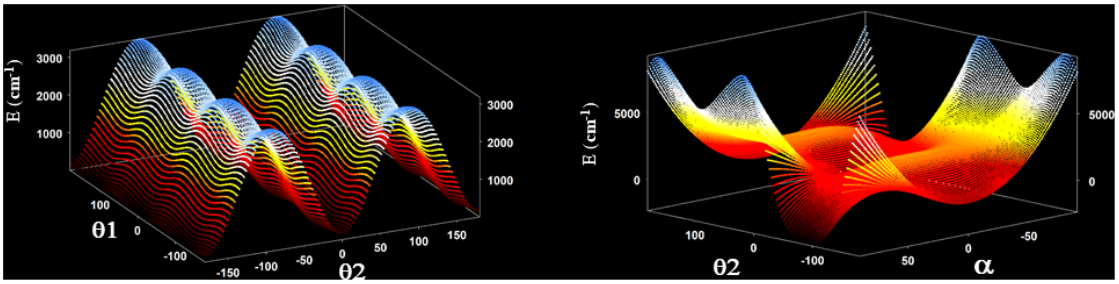

Figure 4. Two dimensional cuts of the 3D potential energy surface of CH_3COCH_2.

Table 10A. Low-lying vibrational energy levels (in cm^{-1})[a] of the CH_3CO, CH_2CHO and CH_3COCH_2 radicals computed variationally or using the vibrational second order perturbation theory. Variational energy levels are classified using the m, n and l quanta corresponding to the θ_1, θ_2, and α coordinates according to the excitation energy. The irreducible representations are given according to the MSG G_6, G_4 and G_{12}, respectively.

CH_3CO (G_6)					CH_2CHO (G_4)					
m	**Variational**		**VPT2**		**n l**	**Variational**		**VPT2**		**Exp. [Ref]**
0	A_1 E	0.0 2.997	ZPVE	-	0 0	A^+ B^+	0.000	ZPVE	-	
1	A_2 E	104.265 76.656	ν_{12}	82	1 0	A^- B^-	398.436	ν_{12}	402	402±4[33]
2	A_1 E	132.180 185.760	$2\nu_{12}$	169				ν_9	495	
3	A_2 E	379.440 272.324	$3\nu_{12}$	261	0 1	A^- B^-	745.727	ν_{11}	729	557[33]
4	A_1 E	379.849 507.146	$4\nu_{12}$	358	2 0	A^+ B^+	792.306	$2\nu_{12}$	782	
			ν_8	464				$\nu_{12}\nu_9$	893	
			$\nu_{12}\nu_8$	549				ν_8	950	
5	A_2 E	821.806 654.566	$5\nu_{12}$	461				ν_{10}	954	
			$2\nu_{12}\nu_8$	639				$2\nu_9$	993	
			$3\nu_{12}\nu_8$	734	1 1	A^+ B^+	1123.980	$\nu_{12}\nu_{11}$	1107	
6	A_1 E	821.807 1008.819	$6\nu_{12}$	-				ν_7	1132	
			ν_7	833	3 0	A^- B^-	1178.128	$3\nu_{12}$	1140	
			ν_{11}	**931**				$\nu_{11}\nu_9$	1225	
			$2\nu_8$	929				$\nu_{12}\nu_8$	1348	
			$\nu_{12}\nu_7$	**915**				$\nu_{12}\nu_{10}$	1357	
			$\nu_{12}\nu_{11}$	**998**				ν_6	**1365**	
								.....		
					0 2	A^+ B^+	1495.772	$2\nu_{11}$	**1459**	

a) Emphasized in bold transitions where important Fermi displacements are predicted.

Table 10B.

CH_3COCH_2 (G_{12})									
m n l	**Variational**		**VPT2**		**m n l**	**Variational**		**VPT2**	
0 0 0	A_1', A_1'' E′, E″	0.000 0.320	ZPVE	-				$\nu_{21}\nu_{19}$	579
1 0 0	A_2', A_2'' E′, E″	84.176 78.053	ν_{21}	77				$\nu_{21}\nu_{13}$	597
2 0 0	A_1', A_1'' E′, E″	126.301 147.464	$2\nu_{21}$	146				$3\nu_{21}\nu_{14}$	622
3 0 0	A_2', A_2'' A_1', A_1'' E′, E″ E′, E″	253.926 255.131 194.827 326.007	$3\nu_{21}$	207				$2\nu_{21}\nu_{19}$	651
0 1 0	A_2', A_2'' E′, E″	327.653 328.917	ν_{20}	343				$2\nu_{21}\nu_{13}$	665
			ν_{14}	385	0 2 0	A_1', A_1'' E′, E″	639.762 639.650	$2\nu_{20}$	683
1 1 0	A_1', A_1'' E′, E″	414.182 407.636	$\nu_{21}\nu_{20}$	410	0 0 1	A_2', A_2'' E′, E″	687.576 686.820	ν_{18}	732
2 1 0	A_2', A_2'' E′, E″	459.559 412.652	$2\nu_{21}\nu_{20}$	468				$\nu_{20}\nu_{14}$	726
			$\nu_{21}\nu_{14}$	472				$3\nu_{21}\nu_{19}$	715
4 0 0	A_1', A_1'' A_2', A_2'' E′, E″ E′, E″	507.358 507.467 479.993 527.420	$4\nu_{21}$	260				$3\nu_{21}\nu_{13}$	725
3 1 0	A_1', A_1'' A_2', A_2'' E′, E″ E′, E″	586.289 587.815 613.918 660.732	$3\nu_{21}\nu_{20}$	519				$2\nu_{20}\nu_{21}$	739
			ν_{19}	500		.....			
			$2\nu_{21}\nu_{14}$	551	0 0 2	A_1', A_1''	1387.228	$2\nu_{18}$	1459
			ν_{13}	521					

a) Emphasized in bold transitions where important Fermi displacements are predicted.

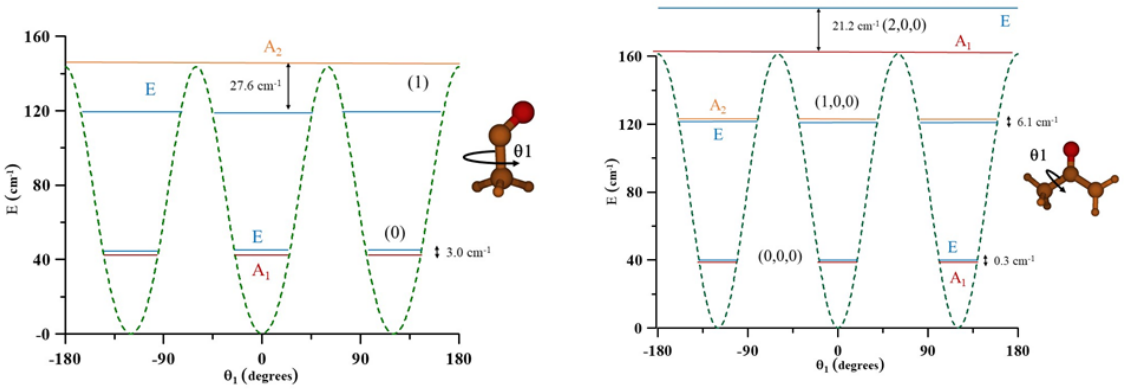

Figure 5. Methyl torsional energy levels of CH_3CO and CH_3COCH_2.

states) was very small due to the height of the torsional barrier V_2=3838.7 cm^{-1}. For CH_2CHO, the VPT2 model seems to be valid.

In CH_3COCH_2, the A/E CH_3 torsional splitting of the ground vibrational state was computed to be 0.320 cm^{-1}. The two components of the three fundamentals ν_{21} (1 0 0 ←0 0 0), ν_{20} (0 1 0 ←0 0 0), and ν_{18} (0 0 1 ←0 0 0), were computed to be 84.176/77.733 cm^{-1}, 327.653/328.597 cm^{-1}, and 687.576/686.500 cm^{-1}, respectively.

Conclusions

All the possible acetone formation routes starting from 58 selected reactants were automatically generated by the programme STAR. This analysis resulted in 75 exergonic processes involving CH_3, CH_3CO and CH_3COCH_2 radicals of which only 14 went through one or two steps and only two of them could be considered barrierless processes. The latter are the addition process H+ CH_3COCH_2 and CH_3+CH_3CO. Both showed similar kinetic rates. The 75 exergonic processes are collected in Table 11. Figure 6 shows the profiles of the fourteen simplest exergonic reactions processes.

Table 11. Exergonic reactions with reactants (ΔG, in kcal/mol, at 10K and 0.1atm at CBS-QB3 level of theory; MNES is the maximum number of necessary elementary steps).

	Reactions	ΔG	MNES
1	$H^\bullet + CH_3COCH_2 \rightarrow CH_3COCH_3$	-94,9	1
2	$CH_3^\bullet + CH_3CO^\bullet \rightarrow CH_3COCH_3$	-83,4	1
3	$CH_3^\bullet + {}^\bullet CH_2CHO \rightarrow CH_3COCH_3$	-89,2	2
4	$HCO^\bullet + CH_3COCH_2 \rightarrow CH_3COCH_3 + CO$	-80,6	2
5	$CH_3O^\bullet + CH_3COCH_2 \rightarrow CH_3COCH_3 + H_2CO$	-75,8	2
6	$CH_2OH^\bullet + CH_3COCH_2 \rightarrow CH_3COCH_3 + H_2CO$	-67,3	2
7	$CHOH + CH_3COCH_2 \rightarrow CH_3COCH_3 + HCO^\bullet$	-60,3	2
8	$^\bullet CH_2CHO + CH_3COCH_2 \rightarrow CH_3COCH_3 + CH_2CO$	-59,1	2
9	$CH_3CO^\bullet + CH_3COCH_2 \rightarrow CH_3COCH_3 + CH_2CO$	-53,3	2
10	$HOCO+ + CH_3CCH_3 \rightarrow CH_3COCH_3 + HOC+$	-32,3	2
11	$HC_2CHO + CH_3CCH_3 \rightarrow CH_3COCH_3 + l\text{-}C_3H_2$	-24,0	2
12	$l\text{-}H_2C_4 + CH_3COCH_2 \rightarrow CH_3COCH_3 + C_4H^\bullet$	-8,9	2
13	$H_2CO+CH_3COCH_2 \rightarrow CH_3COCH_3 + HCO^\bullet$	-7,4	2
14	$l\text{-}C_3H_2 + CH_3COCH_2 \rightarrow CH_3COCH_3 + l\text{-}C_3H^\bullet$	-4,6	2
15	$^3CH_2+CH_3CHO \rightarrow CH_3COCH_3$	-104,9	3
16	$CH_2CO+CH_3CHO \rightarrow CH_3COCH_3 + CO$	-27,2	4
17	$CH_4 + CH_2CO \rightarrow CH_3COCH_3$	-21,1	4
18	$CH_3O^\bullet + CH_3CHOH \rightarrow CH_3COCH_3 + H_2O$	-101,5	4
19	$CH_2OH^\bullet + CH_3CHOH \rightarrow CH_3COCH_3 + H_2O$	-92,9	4
20	$CH_2OH^\bullet + CH_3CCH_3 \rightarrow CH_3COCH_3 + CH_3^\bullet$	-86,5	4
21	$CH_2CHOH + CH_3CCH_3 \rightarrow CH_3COCH_3 + C_2H_4$	-83,0	4
22	$CH_3^\bullet + CH_3CHOH \rightarrow CH_3COCH_3 + H_2$	-75,3	4
23	$CH_3CHO + CH_3CCH_3 \rightarrow CH_3COCH_3 + C_2H_4$	-72,4	4
24	$HOCO^\bullet + CH_3CCH_3 \rightarrow CH_3COCH_3 + HCO^\bullet$	-71,2	4
25	$HOCO+ + CH_3CCH_3 \rightarrow CH_3COCH_3 + HCO+$	-70,0	4
26	$HCOOH + CH_3CCH_3 \rightarrow CH_3COCH_3 + H_2CO$	-61,5	4
27	$CHOH + CH_3CCH_3 \rightarrow CH_3COCH_3 + {}^3CH_2$	-57,2	4
28	$CH_3COOH + CH_3CCH_3 \rightarrow CH_3COCH_3 + CH_2CHOH$	-51,1	4
29	$CH_3O^\bullet + CH_3CHCH_2 \rightarrow CH_3COCH_3 + CH_3^\bullet$	-27,4	4

	Reactions	ΔG	MNES
30	$C_6H^{\bullet} + CH_3CHOH \rightarrow CH_3COCH_3 + C_5$	-26,5	4
31	$CH_3OH + CH_3CHO \rightarrow CH_3COCH_3 + H_2O$	-21,7	4
32	$OH^{\bullet} + CH_3CHCH_2 \rightarrow CH_3COCH_3 + H^{\bullet}$	-14,8	4
33	$CH_3O^{\bullet} + CH_3CHO \rightarrow CH_3COCH_3 + OH^{\bullet}$	-7,7	4
34	$CH_3CHO + {}^{\bullet}CH_2CHO \rightarrow CH_3COCH_3 + HCO^{\bullet}$	-5,7	4
35	$CH_3CHO + CH_3CHCH_2 \rightarrow CH_3COCH_3 + C_2H_4$	-4,7	4
36	$CH_3CHO + CH_3CHOH \rightarrow CH_3COCH_3 + CH_2OH^{\bullet}$	-2,8	4
37	$CH_3CCH + CH_3CHO \rightarrow CH_3COCH_3 + C_2H_2$	-1,8	4
38	$CH^{\bullet} + CH_3CHOH \rightarrow CH_3COCH_3$	-179,6	5
39	$CH_3OH + CH_3CCH_3 \rightarrow CH_3COCH_3 + CH_4$	-94,9	5
40	$HOCO^{\bullet} + CH_3COCH_2 \rightarrow CH_3COCH_3 + CO_2$	-94,6	2
41	$^3CH_2 + CH_3CHOH \rightarrow CH_3COCH_3 + H^{\bullet}$	-80,8	5
42	$H_2O + CH_3CCH \rightarrow CH_3COCH_3$	-37,8	5
43	$l\text{-}C_3H_2 + CH_3CHOH \rightarrow CH_3COCH_3 + C_2H^{\bullet}$	-35,9	5
44	$C_4H^{\bullet} + CH_3CHOH \rightarrow CH_3COCH_3 + C_3$	-33,8	5
45	$H_2C_6 + CH_3CHOH \rightarrow CH_3COCH_3 + C5H^{\bullet}$	-32,7	5
46	$CH_2CO + CH_3COOH \rightarrow CH_3COCH_3 + CO_2$	-31,7	5
47	$C_2H_2 + CH_3COOH \rightarrow CH_3COCH_3 + CO$	-30,7	5
48	$CH_3OH + CH_3CHCH_2 \rightarrow CH_3COCH_3 + CH_4$	-27,3	5
49	$l\text{-}H_2C_4 + CH_3COOH \rightarrow CH_3COCH_3 + C_3O$	-24,8	5
50	$CH_2OH\bullet + CH_3CHCH_2 \rightarrow CH_3COCH_3 + CH_3^{\bullet}$	-18,8	5
51	$CH_2CHOH + CH_3CO^{\bullet} \rightarrow CH_3COCH_3 + HCO^{\bullet}$	-10,5	5
52	$^3CH_2 + CH_3CH_2OH \rightarrow CH_3COCH_3 + H_2$	-91,4	6
53	$C_2H_4 + CHOH \rightarrow CH_3COCH_3$	-89,9	6
54	$CH^{\bullet} + CH_3CH_2OH \rightarrow CH_3COCH_3 + H\bullet$	-85,7	6
55	$CHOH + CH_3CHOH \rightarrow CH_3COCH_3 + OH^{\bullet}$	-55,6	6
56	$l\text{-}H_2C_4 + CH_3CHOH \rightarrow CH_3COCH_3 + l\text{-}C_3H^{\bullet}$	-22,6	6
57	$CH_2OHCHO + CH_3CO^{\bullet} \rightarrow CH_3COCH_3 + OHCO^{\bullet}$	-17,4	6
58	$CH_2CO + CH_3CHOH \rightarrow CH_3COCH_3 + HCO^{\bullet}$	-17,4	6
59	$C_2H_4 + CH_3CHOH \rightarrow CH_3COCH_3 + CH_3^{\bullet}$	-16,9	6
60	$CH_2CHOH + CH_3CHCH_2 \rightarrow CH_3COCH_3 + C_2H_4$	-15,3	6
61	$l\text{-}C_3H^{\bullet} + CH_3CHOH \rightarrow CH_3COCH_3 + C_2$	-14,7	6
62	$CH_2CHOH + CH_3CHOH \rightarrow CH_3COCH_3 + CH_2OH^{\bullet}$	-13,4	6
63	$CH_2OHCHO + CH_3CHCH_2 \rightarrow CH_3COCH_3 + CH_2CHOH$	-10,4	6
64	$CH_3CCH + CH_3COOH \rightarrow CH_3COCH_3 + CH_2CO$	-5,3	6
65	$H_2CO + CH_3CHOH \rightarrow CH_3COCH_3 + OH^{\bullet}$	-2,7	6
66	$HOCO^{+} + CH_3CHCH_2 \rightarrow CH_3COCH_3 + HCO^{+}$	-2,4	6
67	$H_2CO + C_2H_4 \rightarrow CH_3COCH_3$	-36,8	7
68	$CH_3CH_2OH + CHCO \rightarrow CH_3COCH_3 + HCO^{\bullet}$	-28,5	7
69	$CH_3O^{\bullet} + C_2H_4 \rightarrow CH_3COCH_3 + H^{\bullet}$	-17,7	7
70	$CH_2CHOH + CH_3CHOH \rightarrow CH_3COCH_3 + CH_3O^{\bullet}$	-4,8	7
71	$H_2O + CH_3CHCH_2 \rightarrow CH_3COCH_3 + H_2$	-1,3	7
72	$C_2H_2 + CH_3OH \rightarrow CH_3COCH_3$	-57,8	8
73	$CH_2OHCHO + CH_3CHCH_2 \rightarrow CH_3COCH_3 + CH_3CHO$	-21,0	8
74	$C_2H_4 + CH_3OH \rightarrow CH_3COCH_3 + H_2$	-18,2	8
75	$CH_2OH^{\bullet} + C_2H_4 \rightarrow CH_3COCH_3 + H^{\bullet}$	-9,2	8

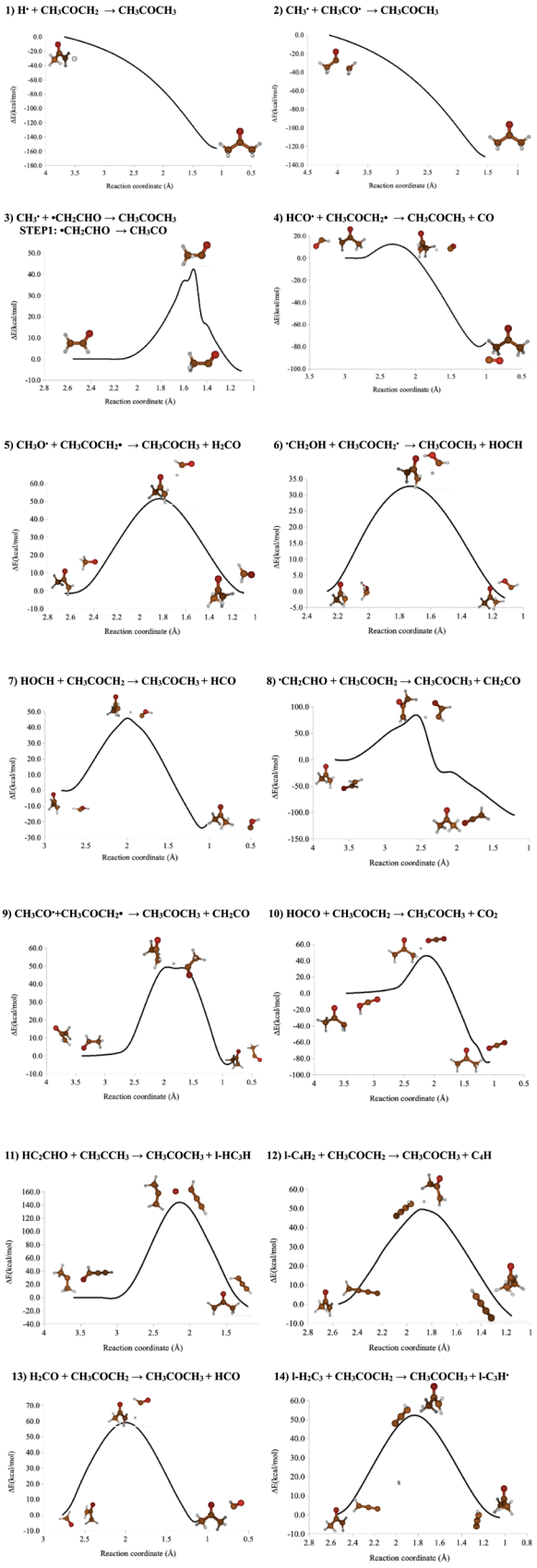

Figure 6. Minimum Energy Paths (MEP) corresponding to the formation processes of acetone computed at the M052X/6-31+G(d.p) level of theory.

The geometrical and spectroscopic properties of some radicals involved in the processes, i.e. CH_3CO, its isomer CH_2CHO, and CH_3COCH_2, were determined by combining the two procedures and various levels of electronic structure theory. The first order properties such as geometries, equilibrium rotational constants, and harmonic fundamentals were determined using RCCSD(T). Using VPT2 and three MP2 anharmonic force fields, centrifugal distortion constants and anharmonic corrections for the spectroscopic parameters were computed.

As the three radicals are nonrigid species, the far infrared region was explored using a variational procedure depending on 1, 2, and 3 independent coordinates. Potential energy surfaces were computed at the RCCSD(T) levels of theory and were vibrationally corrected using MP2. This procedure takes into consideration the interconversion of the minima and allows to determine torsional splittings. In CH_3CO, the A_1/E splitting of the ground vibrational state, was evaluated to be 2.997 cm^{-1}, as was expected given the very low torsional barrier (V_3=143.7 cm^{-1})**.**The methyl torsional fundamental ν_{12} (1←0) computed to be 82 cm^{-1} with VPT2, presented two components to be 104.265 cm^{-1} (A_2←A_1) and 73.659 cm^{-1} (E←E). In CH_2CHO, the two independent fundamentals ν_{12} (1 0←0 0) and ν_{11} (0 1←0 0) were computed to be ν_{12} =398.436 cm^{-1} (A^-←A^+, B^-←B^+) and ν_{11} =745.727 cm^{-1} (A^-←A^+, B^-←B^+). The separation between splitting components is very small due to the height of the torsional barrier V_2=3838.7 cm^{-1}. For CH_2CHO, the VPT2 model seems to be valid. In CH_3COCH_2, the A/E CH_3 torsional splitting of the ground vibrational state was computed to be 0.320 cm^{-1}. The two components of the three fundamentals ν_{21} (1 0 0 ←0 0 0), ν_{20} (0 1 0 ←0 0 0), and ν_{18} (0 0 1 ←0 0 0), were computed to be 84.176/77.733 cm^{-1}, 327.653/328.597 cm^{-1}, and 687.576/686.500 cm^{-1}, respectively.

Data availability

Underlying data

All data underlying the results are included within the manuscript and no additional data are required.

References

1. Mellouki A, Wallington TJ, Chen J: **Atmospheric chemistry of oxygenated volatile organic compounds: impacts on air quality and climate.** *Chem Rev.* 2015; **115**(10): 3984–4014.
PubMed Abstract | Publisher Full Text
2. Atkinson R, Arey J: **Atmospheric degradation of volatile organic compounds.** *Chem Rev.* 2003; **103**(12): 4605–4638.
PubMed Abstract | Publisher Full Text
3. Singh HB, O'Hara D, Herlth D, *et al.*: **Acetone in the atmosphere: distribution, sources, and sinks.** *JGR Atmospheres.* 1994; **99**(D1): 1805–1819.
Publisher Full Text
4. Combes F, Gerin M, Wootten A, *et al.*: **Acetone in interstellar space.** *Astron Astrophys.* 1987; **180**: L13–L16.
Reference Source
5. Snyder LE, Lovas FJ, Mehringer DM, *et al.*: **Confirmation of interstellar acetone.** *Astrophys J.* 2002; **578**(1): 245–255.
Publisher Full Text
6. Folkins I, Chatfield R: **Impact of acetone on ozone production and OH in the upper troposphere at high NO_x.** *JGR-Atmospheres.* 2000; **105**(D9): 11585–11599.
Publisher Full Text
7. Caralp F, Forst W, Hénon E, *et al.*: **Tunneling in the reaction of acetone with OH.** *Phys Chem Chem Phys.* 2006; **8**(9): 1072–1078.
PubMed Abstract | Publisher Full Text
8. Fuente A, Cernicharo J, Caselli P, *et al.*: **The hot core towards the intermediate-mass protostar NGC 7129 FIRS 2.** *Astron Astrophys.* 2014; **568**(A&A): A65–A94.
Publisher Full Text
9. Lykke JM, Coutens A, Jørgensen JK, *et al.*: **The ALMA-PILS survey: First detections of ethylene oxide, acetone and propanal toward the low-mass protostar IRAS 16293-2422.** *Astron Astrophys.* 2017; **597**(A&A): 53–88.
Publisher Full Text
10. Skouteris D, Balucani N, Ceccarelli C, *et al.*: **The Genealogical Tree of Ethanol: Gas-phase Formation of Glycolaldehyde, Acetic Acid, and Formic Acid.** *Astrophys J.* 2018; **854**(2): 135–144.
Publisher Full Text
11. Gámez V, Senent ML: **The formation of $C_3O_3H_6$ structural isomers in the gas phase through barrierless pathways. Formation and spectroscopic characterization of methoxy acetic acid.** *Astrophys J.* 2021; **913**: 21–37.
Publisher Full Text
12. Senent ML, Moule DC, Smeyers YG, *et al.*: **A Theoretical Spectroscopic Study of the $\tilde{A}^1A_u(S_1) \leftarrow \tilde{X}^1A_g(S_0)$, $n \rightarrow \pi^*$ Transition in Biacetyl, $(CH_3CO)_2$.** *J Mol Spectrosc.* 1994; **164**: 66–78.
Publisher Full Text
13. Senent ML, Dalbouha S: **Large amplitude motions of pyruvic acid (CH_3-CO-COOH).** Molecules, "Terahertz spectroscopy and dynamics of low-frequency modes involving large amplitude molecular motions. *Molecules.* MDPI, 2021; **26**(14): 4269–4282.
PubMed Abstract | Publisher Full Text | Free Full Text
14. Hirota E, Mizoguchi A, Ohshima Y, *et al.*: **Interplay of methyl-group internal rotation and fine and hyperfine interaction in a free radical: Fourier transform microwave spectroscopy of the acetyl radical.** *Mol Phys.* 2007; **105**(5–7): 455–466.
Publisher Full Text
15. Endo Y, Nakajima M: **Fourier-transform microwave spectroscopy of the vinoxy radical, CH_2CHO.** *J Mol Spectrosc.* 2014; **301**: 15–19.
Publisher Full Text
16. Hansen N, Mäder H, Temps F: **Rotational transitions of the CH_2CHO radical detected by pulsed laser photolysis–molecular beam–Fourier-transform microwave spectroscopy.** *J Mol Spectrosc.* 2001; **209**(2): 278–279.
Publisher Full Text
17. Jacox ME: **The reaction of F atoms with acetaldehyde and ethylene oxide. Vibrational spectra of the CH_3CO and CH_2CHO free radicals trapped in solid argon.** *J Chem Phys.* 1982; **69**(3): 407–422.
Publisher Full Text
18. Shirk JS, Pimentel GC: **Potential functions and the bonding in the XCO free radicals.** *J Am Chem Soc.* 1968; **90**(13): 3349–3351.
Publisher Full Text
19. Lin MY, Huang TP, Wu PZ, *et al.*: **Infrared spectra of the 1-methylvinoxide radical and anion isolated in solid argon.** *J Phys Chem A.* 2019; **123**(22): 4750–4754.
PubMed Abstract | Publisher Full Text
20. Das P, Lee YP: **Bimolecular reaction of CH_3 + CO in solid *p*-H_2:**

infrared absorption of acetyl radical (CH_3CO) and CH_3-CO complex. *J Chem Phys.* 2014; **140**(24): 244303.
PubMed Abstract | Publisher Full Text

21. Utkin YG, Han JX, Sun F, *et al.*: **High-resolution jet-cooled and room temperature infrared spectra of the ν_3 CH stretch of vinoxy radical.** *J Chem Phys.* 2003; **118**(23): 10470–10476.
Publisher Full Text

22. Inoue G, Akimoto H: **Laser-induced fluorescence of the C_2H_3O radical.** *J Chem Phys.* 1981; **74**(1): 425–433.
Publisher Full Text

23. DiMauro LF, Heaven M, Miller TA: **Laser induced fluorescence study of the $B^2A'' \rightarrow X\ ^2A''$ transition of the vinoxy radical in a supersonic free jet expansion.** *J Chem Phys.* 1984; **81**(5): 2339–2346.
Publisher Full Text

24. Wan R, Chen X, Wu F, *et al.*: **Observation of new vibronic transitions in the B^2 A''–X^2 A'' manifold of the CH_2CHO radical.** *J Chem Phys Lett.* 1996; **260**(5–6): 539–544.
Publisher Full Text

25. Brock LR, Rohlfing EA: **Spectroscopic studies of the B $^2A''$ -X $^2A''$ system of the jet-cooled vinoxy radical.** *J Chem Phys.* 1997; **106**(24): 10048–10065.
Publisher Full Text

26. Yacovitch TI, Garand E, Neumark DM: **Slow photoelectron velocity-map imaging spectroscopy of the vinoxide anion.** *J Chem Phys.* 2009; **130**(24): 244309.
PubMed Abstract | Publisher Full Text

27. Mead RD, Lykke KR, Lineberger WC: **Spectroscopy and dynamics of the dipole-bound state of acetaldehyde enolate.** *J Chem Phys.* 1984; **81**(11): 4883–4892.
Publisher Full Text

28. Yacovitch TI, Garand E, Neumark DM: **Slow photoelectron velocity-map imaging of the *i*-methylvinoxide anion.** *J Phys Chem A.* 2010; **114**(42): 11091–11099.
PubMed Abstract | Publisher Full Text

29. Rajakumar B, Flad JE, Gierdzak T, *et al.*: **Visible absorption spectrum of the CH_3CO radical.** *J Phys Chem A.* 2007; **111**(37): 8950–8958.
PubMed Abstract | Publisher Full Text

30. Adachi H, Basco N, James DGL: **The acetyl radical studied by flash photolysis and kinetic spectroscopy.** *J Chem Phys Lett.* 1978; **59**(3): 502–505.
Publisher Full Text

31. Maricq MM, Szente JJ: **The UV spectrum of acetyl and the kinetics of the chain reaction between acetldehyde and chlorine.** *J Chem Phys Lett.* 1996; **253**(3–4): 333–339.
Publisher Full Text

32. Cameron M, Sivkumaran V, Dillon TJ, *et al.*: **Reaction between OH and CH_3CHO.** *Phys Chem Chem Phys.* 2002; **4**(15): 3628–3638.
Publisher Full Text

33. Hunziker HE, Kneppe H, Wendt HR: **Photochemical modulation spectroscopy of oxygen atom reactions with olefins.** *J Photochem.* 1981; **17**(2): 377–387.
Publisher Full Text

34. Alconcel LS, Deyerl HJ, Zengin V, *et al.*: **Structure and energetics of vinoxide and the X($^2A''$) and A($^2A'$) vinoxy radicals.** *J Phys Chem A.* 1999; **103**(46): 9190–9194.
Publisher Full Text

35. Osborn DL, Choi H, Mordaunt DH, *et al.*: **Fast beam photodissociation spectroscopy and dynamics of the vinoxy radical.** *J Chem Phys.* 1997; **106**(8): 3049–3066.
Publisher Full Text

36. Nagai H, Carter RT, Huber JR: **Spectroscopy and dynamics of selected rotational levels in the B^2 A'' state of the vinoxy radical.** *J Chem Phys Lett.* 2000; **331**(5–6): 425–432.
Publisher Full Text

37. Williams S, Zingher E, Weisshaar JC: **B ← X Vibronic Spectra and B-State Fluorescence Lifetimes of Methylvinoxy Isomers.** *J Phys Chem A.* 1998; **102**(13): 2297–2301.
Publisher Full Text

38. Williams S, Harding LB, Stanton JF, *et al.*: **Barrier to methyl internal rotation of 1-methylvinoxy radical in the X($^2A''$) and B($^2A''$) states: experiment and theory.** *J Phys Chem.* 2000; **104**: 10131–10138.

39. Mao W, Li Q, Kong F, *et al.*: **Ab initio calculations of the electronic states of acetyl radical.** *J Chem Phys Lett.* 1998; **283**(1): 114–118.
Publisher Full Text

40. Yamaguchi M, Inomata S, Washida N: **Multireference configuration interaction calculation of the B^2A''-X^2A'' transition of halogen- and methyl-substituted vinoxy radicals.** *J Phys Chem A.* 2006; **110**(45): 12419–12426.
PubMed Abstract | Publisher Full Text

41. Bennett DI, Butler LJ, Werner HJ: **Comparing electronic structure predictions for the ground state dissociation of vinoxy radicals.** *J Chem Phys.* 2007; **127**(9): 094309.
PubMed Abstract | Publisher Full Text

42. Dalbouha S, Mogren Al-Mogren M, Senent ML: **Rotational and torsional properties of various monosubstituted isotopologues of acetone (CH_3-CO-CH_3) from explicitly correlated ab initio methods.** *ACS Earth & Space Chem.* 2021; **5**(4): 890–899.
Publisher Full Text

43. Yazidi O, Senent ML, Gámez V, *et al.*: ***Ab initio* spectroscopic characterization of the radical CH_3OCH_2 at low temperatures.** *J Chem Phys.* 2019; **150**(19): 194102.
PubMed Abstract | Publisher Full Text

44. Gámez V, Galano A, Patiño-Leyva O, *et al.*: **Searching tool for astrochemical reactions.** STAR v.1.
Reference Source

45. Zhao Y, Schultz NE, Truhlar DG: **Design of density functionals by combining the method of constraint satisfaction with parametrization for thermochemistry, thermochemical kinetics, and noncovalent interactions.** *J Chem Theory Comput.* 2006; **2**(2): 364–82.
PubMed Abstract | Publisher Full Text

46. Krishnan R, Binkley JS, Seeger R, *et al.*: **Self-consistent molecular orbital methods. XX. A basis set for correlated wave functions.** *J Chem Phys.* 1980; **72**(1): 650–54.
Publisher Full Text

47. Frisch MJ, Trucks GW, Schlegel HB, *et al.*: **Gaussian 16, Revision C.01.** Gaussian, Inc., Wallingford CT, 2016.
Reference Source

48. Montgomery JA, Frisch MJ, Ochterski JW, *et al.*: **A complete basis set model chemistry. VI. Use of density functional geometries and frequencies.** *J Chem Phys.* 1999; **110**(6): 2822–2827.
Publisher Full Text

49. Polyrate-version 2017-C, Zheng J, Bao JL, *et al.*: University of Minnesota: Minneapolis, 2017.
Reference Source

50. Knizia G, Adler TB, Werner HJ: **Simplified CCSD(T)-F12 methods: theory and benchmarks.** *J Chem Phys.* 2009; **130**(5): 054104.
PubMed Abstract | Publisher Full Text

51. Werner HJ, Adler TB, Manby FR: **General orbital invariant MP2-F12 theory.** *J Chem Phys.* 2007; **126**(16): 164102.
PubMed Abstract | Publisher Full Text

52. Werner HJ, Knowles PJ, Manby FR, *et al.*: **MOLPRO.** version 2012.1, a package of *ab initio* programs.
Reference Source

53. Kendall RA, Dunning TH, Harrison RJ: **Electron affinities of the first-row atoms revisited. Systematic basis sets and wave functions.** *J Chem Phys.* 1992; **96**(9): 6796–6806.
Publisher Full Text

54. Knowles PJ, Hampel C, Werner HJ: **Coupled cluster theory for high spin, open shell reference wave functions.** *J Chem Phys.* 1993; **99**(7): 5219.
Publisher Full Text

55. Woon DE, Dunning Jr TH: **Gaussian basis sets for use in correlated molecular calculations. V. Core-valence basis sets for boron through neon.** *J Chem Phys.* 1995; **103**(11): 4572–4585.
Publisher Full Text

56. Barone V: **Anharmonic vibrational properties by a fully automated second-order perturbative approach.** *J Chem Phys.* 2005; **122**(1): 14108.
PubMed Abstract | Publisher Full Text

57. Senent ML: ***Ab initio* determination of the torsional spectra of acetic acid.** *Mol Phys.* 2001; **99**(15): 1311–1321.
Publisher Full Text

58. Senent ML: **Determination of the kinetic energy parameters of non-rigid molecules.** *J Chem Phys Lett.* 1998; **296**(3–4): 299–306.
Publisher Full Text

59. Senent ML: ***Ab initio* determination of the roto-torsional energy levels of *trans*-1,3-butadiene.** *J Mol Spectrosc.* 1998; **191**(2): 265–275.
PubMed Abstract | Publisher Full Text

60. Werner HJ, Knowles PJ: **An efficient internally contracted multiconfiguration-reference configuration interaction method.** *J Chem Phys.* 1998; **89**(9): 5803–5814.
Publisher Full Text

61. Knowles PJ, Werner HJ: **An efficient method for the evaluation of coupling coefficients in configuration interaction calculations.** *Chem Phys Lett.* 1988; **145**(6): 514–522.
Publisher Full Text

62. Nyden MR, Petersson GA: **Complete basis set correlation energies. I. The asymptotic convergence of pair natural**

orbital expansions. *J Chem Phys.* 1981; **75**(4): 1843–1862.
Publisher Full Text

63. Georgievskii Y, Klippenstein SJ: **Variable reaction coordinate transition state theory: Analytic results and application to the $C_2H_3+H \rightarrow C_2H_4$ reaction.** *J Chem Phys.* 2003; **118**(12): 5442–5455.
Publisher Full Text

64. Löhle A, Kästner J: **Calculation of reaction rate constants in the canonical and microcanonical ensemble.** *J Chem Theory Comput.* 2018; **14**(11): 5489–5498.
PubMed Abstract | **Publisher Full Text**

65. Georgievskii Y, Klippenstein SJ: **Long-range transition state theory.** *J Chem Phys.* 2005; **122**(19): 194103.
PubMed Abstract | **Publisher Full Text**

66. Boussesi R, Senent ML, Jaïdane N: **Weak intramolecular interaction effects on the torsional spectra of ethylene glycol, an astrophysical species.** *J Chem Phys.* 2016; **144**(16): 164110.
PubMed Abstract | **Publisher Full Text**

67. Motiyenko RA, Margulès L, Senent ML, *et al.*: **Internal rotation of OH group in 4-hydroxy-2-butynenitrile studied by millimeter-wave spectroscopy.** *J Phys Chem A.* 2018; **122**(12): 3163–3169.
PubMed Abstract | **Publisher Full Text**

68. Dalbouha S, Senent ML, Komiha N, *et al.*: **Structural and spectroscopic characterization of Methyl Isocyanate, Methyl Cyanate, Methyl Fulminate, and Acetonitrile N-oxide using highly correlated *ab initio* methods.** *J Chem Phys.* 2016; **145**(12): 124309.
PubMed Abstract | **Publisher Full Text**

69. Bunker R, Jensen P: **Molecular Symmetry and Spectroscopy.** NRC Research Press, Ottawa, 1989.
Reference Source